# Report on the trend analysis of the CAM daily Calibration measurements

*Version 1.0*

P. Gallais, O. Boulade
Service d'Astrophysique, DAPNIA, CEA/Saclay
91 191 Gif-sur-Yvette cedex, France

*September 19, 1998*

# 1 Purpose of the document

The purpose of this document is to report on the long term behaviour of both the SW and LW detectors of ISOCAM, the infrared camera on-board ISO. During the 2.5 years of its in-flight operations, both detectors have performed nominally and their performances in term of responsivity and dark current have been very stable. In order to monitor these parameters, systematic and reproducible sequences of commanding have been designed to perform the relevant calibration measurements.

These daily measurements were executed during the handover and deactivation windows inside roughly every revolution of the spacecraft.

The results presented in this document are not definitive, and part of this work has already been presented at the *ISO detector workshop* (Boulade et Gallais, 1998). Much information has been extracted from the available data and for a large part of it, we can propose a good explanation. However, some of the addressed points are not yet fully understood and remain to be clarified in more detail.

After the presentation of the data acquisition and of the data reduction, the discussion included here can be summarised by the following :

- The sort of routine engineering calibration measurements described here are of great interest to get an idea of the behaviour of the detectors on a long time scale, but cannot be used for reliable direct calibration purposes.
- The end-of-revolution LW flat-field measurements hold a memory of the saturation events which occurred during the revolution with that detector.
- The end-of-revolution dark current measurements are good indicators of the space weather in the vicinity of the Van Allen electron belt.
- The hand-over LW dark measurements appear to decrease throughout the mission. They have been the starting point for the development of the so-called "dark model".
- De-activation flat-fields helped to verify that CAM recovered well after the increase of the OSS temperature due to Earth viewing on Rev.195.
- Flat-field measurements are affected by wheel jitter.
- Reset levels of the LW detector show, in several occurrences, a strong, abrupt, decrease, followed by a slow recovery, not explained for the time being.

# Warning and usual terms

**Warning: All data presented in this document are given in ADUs. They are corrected neither for integration time nor for ADC gain. Usually, the integration time is indicated on the plots, and the gain is given in table 1 for the sequence under consideration.**

- *ADU* means "Analog-to-Digital Unit", i.e. the signal delivered by the Analog-to-Digital converter of ISOCAM
- *CamTU* is the basic time unit of CAM: 1 CamTU $\approx$ 0.14 seconds

| Descr. | Period in orbit | Entr.Wh. | Sel.Wh. | Lens | Filter | $t_i$ * | Gain | N frames |
|---|---|---|---|---|---|---|---|---|
| Dark LW 0.28sec | H/O even rev. since rev 764 | Hole | LW-1 | LGe 1.5 | Dark 3 | 2 | 2 | 365 |
| Dark LW 2sec | Deact. | Hole | LW-1 | LGe 1.5 | Dark 3 | 15 | 2 | 315 |
| | H/O since rev.150 | | | | | | | 330 |
| | H/O odd rev. since rev 764 | | | | | | | 330 |
| Dark LW 5sec | Deact. until rev.125 | Hole | LW-1 | LGe 1.5 | Dark 3 | 36 | 2 | 330 |
| | H/O since rev.150 | | | | | | | 330 |
| | H/O odd rev. since rev 764 | | | | | | | 330 |
| Dark LW 10sec | H/O even rev. since rev 764 | Hole | LW-1 | LGe 1.5 | Dark 3 | 72 | 2 | 240 |
| Dark SW 2sec | Deact. since rev.270 | Hole | SW-1 | LSi 1.5 | Dark 3 | 15 | 2 | 240 |
| Dark SW 6sec | Deact. | Hole | SW-1 | LSi 1.5 | Dark 3 | 43 | 2 | 100 |
| FF SW1 | Deact. | Dark | SW BB | LSi 1.5 | SW1 | 15 | 2 | 75 |
| FF SW3 | Deact. | Dark | SW BB | LSi 1.5 | SW3 | 15 | 2 | 130 |
| FF LW2 | Deact. | Dark | LW BB | LGe 1.5 | LW2 | 15 | 2 | 130 |
| FF LW3 | Deact. | Dark | LW BB | LGe 1.5 | LW3 | 15 | 2 | 75 |

* integration time is in CamTU(s) ($\approx$ 0.14sec).

Table 1: List of measurements done during either the Hand-over (*H/O*) or de-activation (*Deact.*) windows, and their optical configuration.

- *ICD* means "Internal Calibration Device". It consists in an integrating sphere emitting with a black-body-like spectral energy distribution.
- A *Flat Field* is usually used to refer to a uniform extended source of illumination, uniform over the whole surface of the detector. By extension, the term *Flat Field* is used to refer to the image of such a source. Improperly, the term is used to refer to the response of the ISOCAM detectors to the ICD illumination (which is not, strictly speaking, a source of uniform illumination).

# 2 Data acquisition and data reduction

## 2.1 The sequences of measurements

The sequences of measurements during the de-activation and hand-over windows are summarised in table 1. The profiles of all sequences are shown in figure 1.

### 2.1.1 The de-activation sequence

The sequence of measurements in the de-activation window was defined well before launch, tested during both ground-based calibration campaigns and during integration testing of the instrument in the satellite. Since the first version, but before launch, it has been tuned and optimised to fit into the duration of the window and to allow the signals at the end of each measurement to reach stabilised values.

It has been reviewed only once when the need of frequent dark current measurements for the SW detector at 2 sec integration time appeared. This measurement replaced the dark current measurement of the LW channel at 5 sec integration, the last one being already

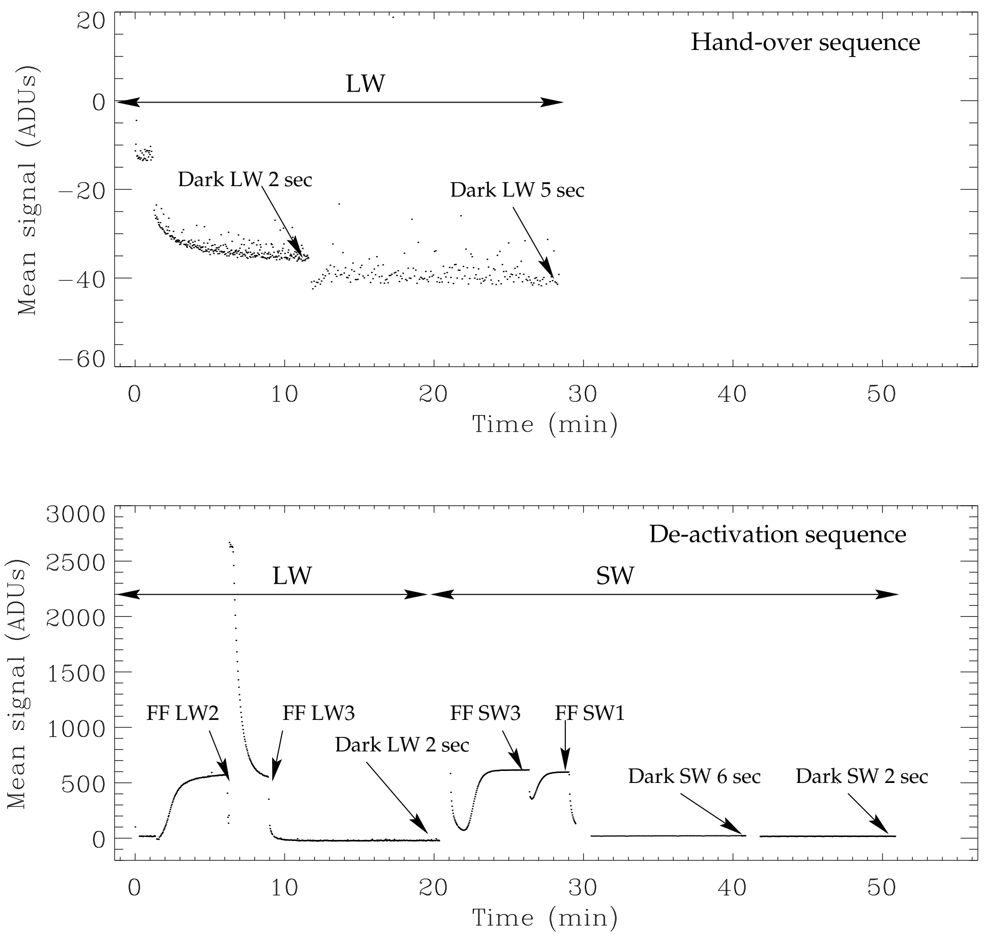


Figure 1: Profiles of the hand-over and de-activation sequences, illustrated by the mean signal over the prime detector versus times since the beginning of the sequence. The arrows indicate which time periods have been considered for the extraction of "assumed stabilized data" for the analysis.

obtained during the hand-over calibrations. This first change has been implemented for revolution 270.

The time window is split into two parts in which the sequences of measurement are built with similar profiles, the first part being reserved for the LW channel, the second one for the SW channel. In each part, and in order to deal with stabilised levels, the flat-field measurements are first performed through 2 filters (LW2 then LW3 for the LW channel, SW3 then SW1 for the SW channel). Then, the Internal Calibration Device (ICD) is switched off and dark current configurations are set.

### 2.1.2 The hand-over sequence

We took advantage of the 30 minutes of the hand-over window during which no science measurements were scheduled. In that window dark measurements for the LW detector have been programmed. The automatic scheduling of these measurements took place on revolution 150. The sequence has been reviewed late in the mission in order to extend the set of measurements of LW dark current to the 0.28 sec and 10 sec integration times. Starting from revolution 764 onwards, dark measurements for the 0.28 sec and 10 sec integration times were automatically scheduled in the hand-over sequences of revolutions with even numbers while the 2 sec and 5 sec integration times remained executed during hand-over sequences of revolutions with odd numbers.

### 2.1.3 Statistics on the whole sample

We dispose for the present analysis, and for each type of measurement, of very complete samples (except for the latest LW dark measurements made inside the hand-over window). 91.8% of the data from de-activation sequences of routine phase (since revolution 79) are available in the archive of the mission. The missing 8.4% have 2 explanations: engineering planned operations (53 revolutions), and contingencies (13 revolutions). 98.6% of the hand-over sequences have been executed. This sequence failed for only 10 revolutions, the reasons being mainly the occurrences of telemetry drops during this period in the revolutions.

## 2.2 Data reduction

Data are extracted from the ISO archive at the SPD (Standard Data Product) level. All data sets have been derived by OLP (Off Line Processing) with a version of this software later than version 6. This allows us to dispose of a set of consistent and homogeneous data which will be reduced always following the same procedure. Data are sliced using CIA (CAM Interactive Analysis) and analysed with specific IDL procedures.

### 2.2.1 Dark current measurements

From the cube of images obtained in the one configuration of the instrument, we derive a dark current measurement image. First, glitches are removed using the so-called TCOR method (see M. Delaney, 1998). To be free of the non-stabilised data, only the last images of the cube, which are well stabilised, are considered to compute a mean dark current measurement.

Then, for each revolution and for each type of dark, an image is obtained, and a cube of mean images is built along the whole mission. From this cube, a median dark image is derived, which can be used as a "reference" (for comparison) measurement for the whole set.

In parallel, the temporal rms noise of each pixel of the image in the sequence is computed and we derive the mean temporal noise over the whole array.

### 2.2.2 Flat-Field measurements

The basic processing is very close to the one applied to reduce dark current measurements. The only difference is that only the last frames of the sequence, which are well stabilised, are kept to compute the mean image of the responsivity under ICD illumination.

All images are corrected for dark current using the image of dark current obtained during the de-activation sequence of the revolution. However, if such a dark is not available (case of SW flat-field until revolution 270), the derived median dark current image is used instead. Then a median responsivity image for the whole mission is derived which will be used as reference for the whole set of flat-field measurements over the mission, in the trend analysis context.

# 3 General trends of basic parameters

## 3.1 SW channel

### 3.1.1 Dark current measurements

The levels and noise of the SW dark current measurements are displayed in figures 2 and 3, respectively for 2 seconds and 6 seconds integration times. The levels stayed very stable over the whole duration of the mission. The spikes seen in both the signal and the noise curves can be explained by the variation of the electron fluence in the vicinity of the radiation belts. This point is discussed in more detail in Boulade et Gallais (1998) and also in section 4.1 of this document. Despite this feature, the evolution of the dark level can be derived from the baseline of the curves. It evolved, decreasing smoothly by 0.36 and 0.16 ADUs/100 revolutions respectively for 2 and 6 sec integration times. The noise for both measurements presents variations of 3% of the dark level, variations which have no explanation for the time being.

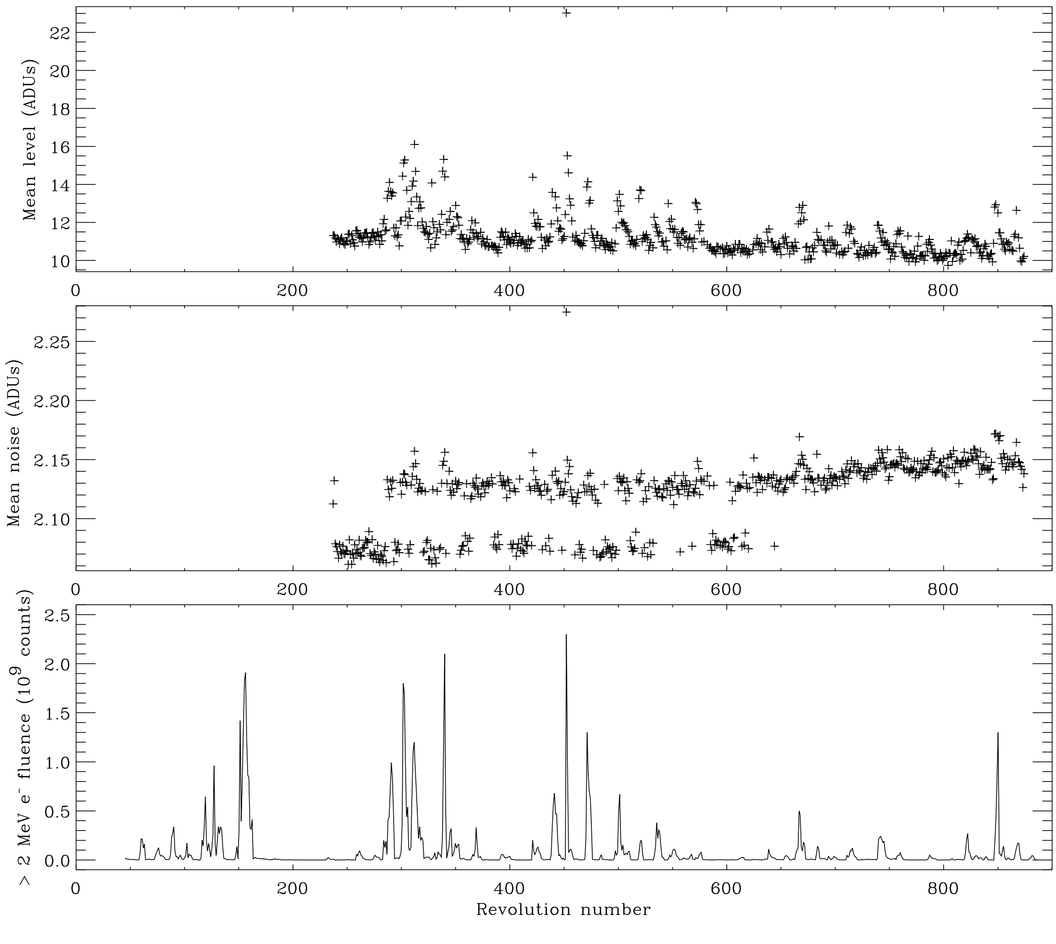


Figure 2: Deactivation SW 2 sec dark current measurements: mean level (top), mean temporal noise (middle). The bottom plot displays the GOES-9 electron fluence which can explain the spikes of the dark current measurements (see section 4.1).

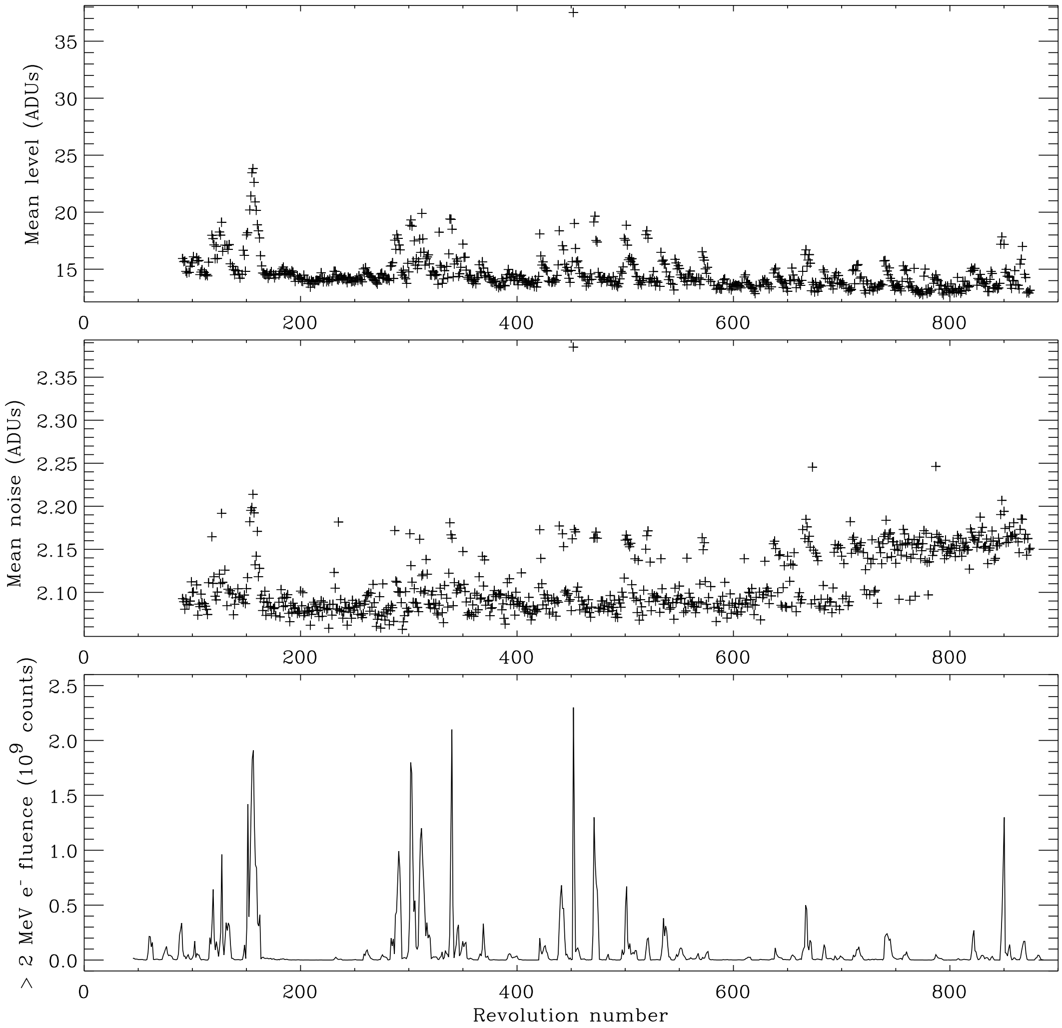


Figure 3: Deactivation SW 6 sec dark current measurements: mean level (top), mean temporal noise (middle). The bottom plot displays the GOES-9 electron fluence which can explain the spikes of the dark current measurements (see section 4.1).

### 3.1.2 Responsivity

The responsivity curves of the SW detector to signal produced by the ICD is shown on figures 4 and 5 respectively, for measurements through SW1 and SW3 filters. The shapes of both measurements are similar. The multi-modal distributions of the points seen on these graphs are due to wheel jitter (see section 4.2 in which we try to remove this splitting). Despite this distribution, the envelopes of the curves show that the responsivity has been quite stable throughout the mission, with a decrease of no more than 0.5% over the whole mission. This measurement must be seen as deriving from the combination of a chain of elements, the main ones being the detector on one side and the ICD on the other. Therefore, we must keep in mind that it is impossible to discriminate any evolution of the detector responsivity from an evolution of the ICD emissivity.

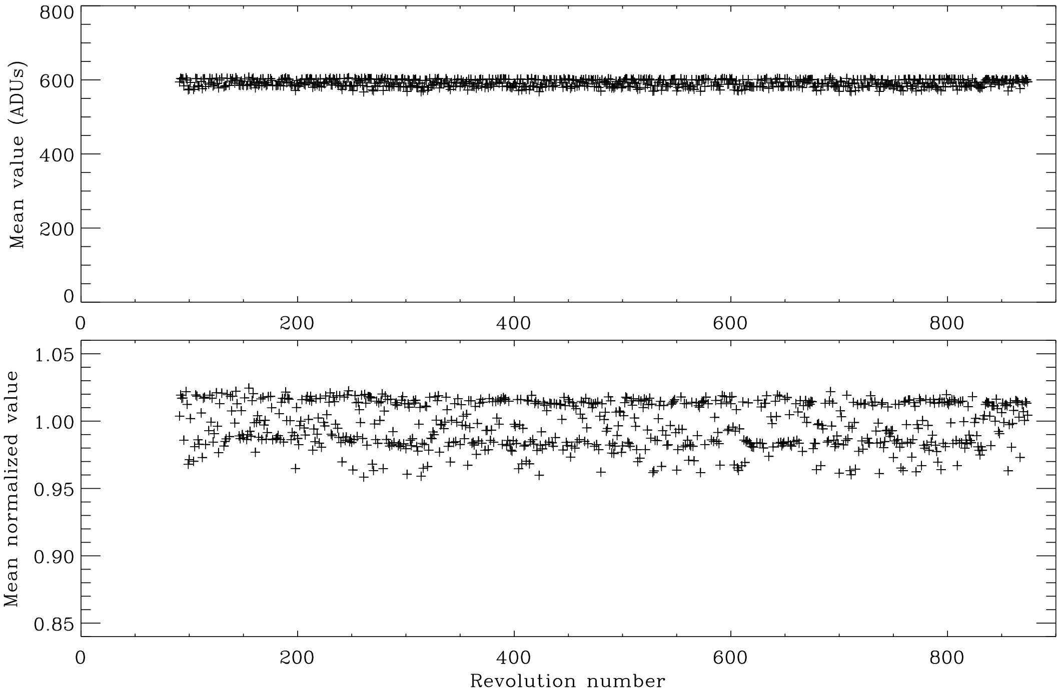


Figure 4: SW responsivity through SW1 filter from deactivation measurements: mean level (top), mean normalized value (bottom).

## 3.2 LW channel

### 3.2.1 Dark current measurements

The LW dark current levels and noise are displayed on figures 6, 7 and 8. As for the SW channel, the deactivation dark measurements are highly sensitive to the space weather in the vicinity of the radiation belts (see section 4.1). However, it is clearly seen on the base line that the level decreases continuously from the beginning of the mission. This trend is also seen in the hand-over measurements. The level of the dark at 2 seconds integration time has decreased by about 4 ADUs over the whole mission and the one obtained at 5 seconds integration time has decreased by about 3.5 ADUs over the whole mission. In addition, the pattern of the dark on the array has changed, the behaviour of the odd and even lines being different (see Biviano et al, 1997).

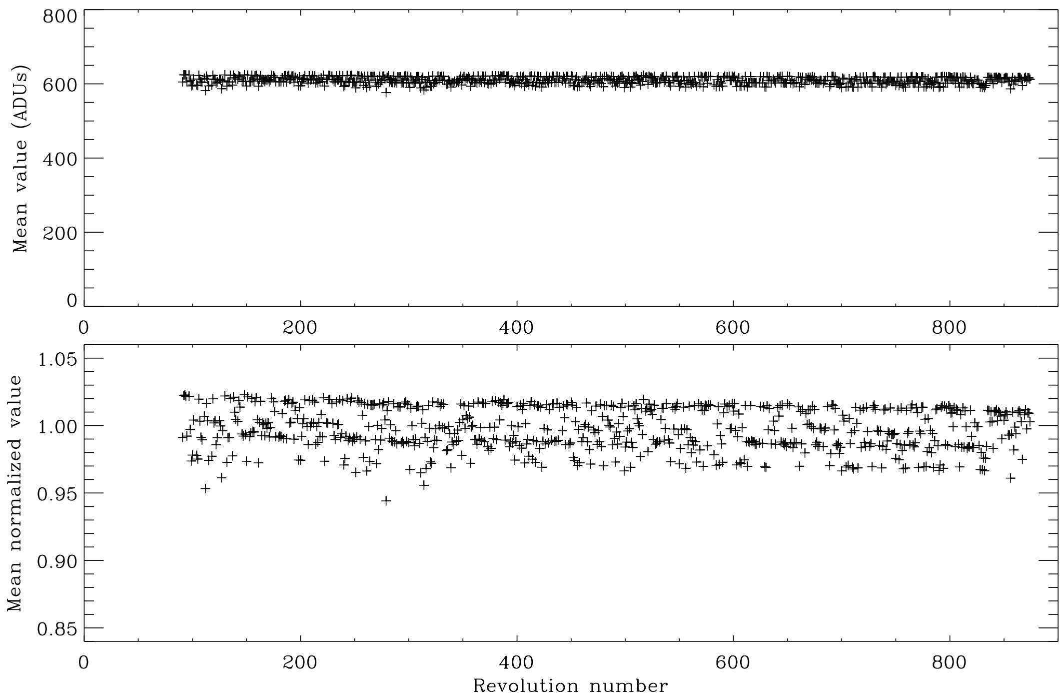


Figure 5: SW responsivity through SW3 filter from deactivation measurements: mean level (top), mean normalized value (bottom).

The trends of the LW dark current then must be taken into account for data reduction. If this is not done, then a striped pattern (linked to the parity of the lines) will remain on the images at the 1 to 2 ADU level. A model has been developed to take into account the trends of the dark both through the mission and along the orbit (Biviano et al, 1997), which provides a very good dark current correction for all integration times used with the LW detector.

### 3.2.2 Responsivity

The responsivity of the LW channel through LW2 and LW3 filters, under ICD illumination, throughout the mission, are shown in figures 9 and 10. While the responsivity through the LW2 filter is characterized by a slow decrease along the mission (at the rate of 0.8% per 100 revolutions), the mean responsivity through the LW3 filter is more chaotic but shows also such a decrease, a little bit steeper around the end of the mission. Once again, it is quite difficult to distinguish the trend of the responsivity of the detector from the trend of the ICD emissivity, and the present measurements must be taken as a characterisation of the global chain.

As for the SW flat-fields, but at a lower level, the LW flat-fields are also affected by wheel jitter (see section 4.2).

Annex A gives for each revolution, the deviation of the LW2 flat-field from the median flat-field derived from the whole set of measurements. On a non-negligable number of images, a pattern can be seen, different from one image to another, and clearly identified as a remnant of a saturation event which occured earlier in the revolution. For more details, this topic is addressed in section 4.3. The wheel jitter and the saturation remnants contribute strongly to the dispersion of the mean flat-field measurements.

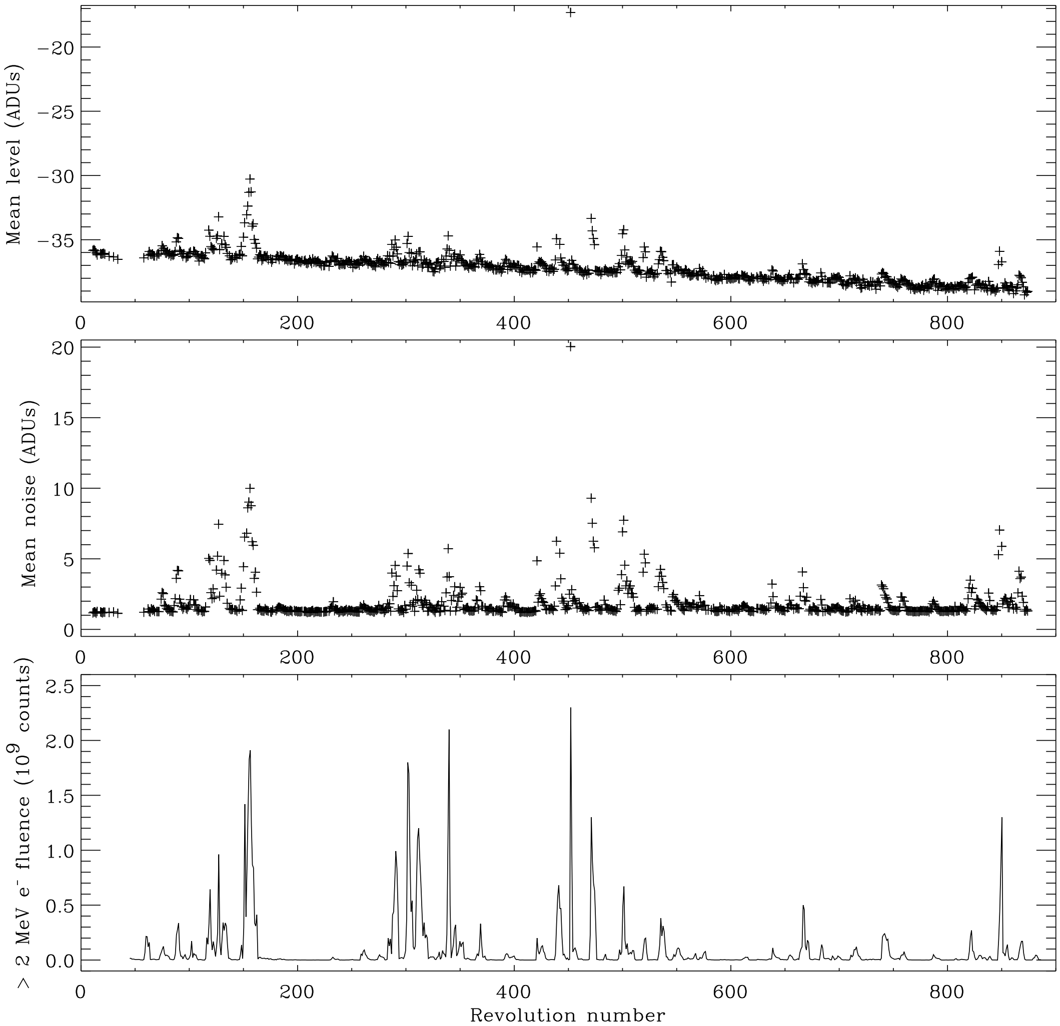


Figure 6: Deactivation LW 2 sec dark current measurements: mean level (top), mean temporal noise (middle). The bottom plot displays the GOES-9 electron fluence which can explain the spikes of the dark current measurements (see section 4.1).

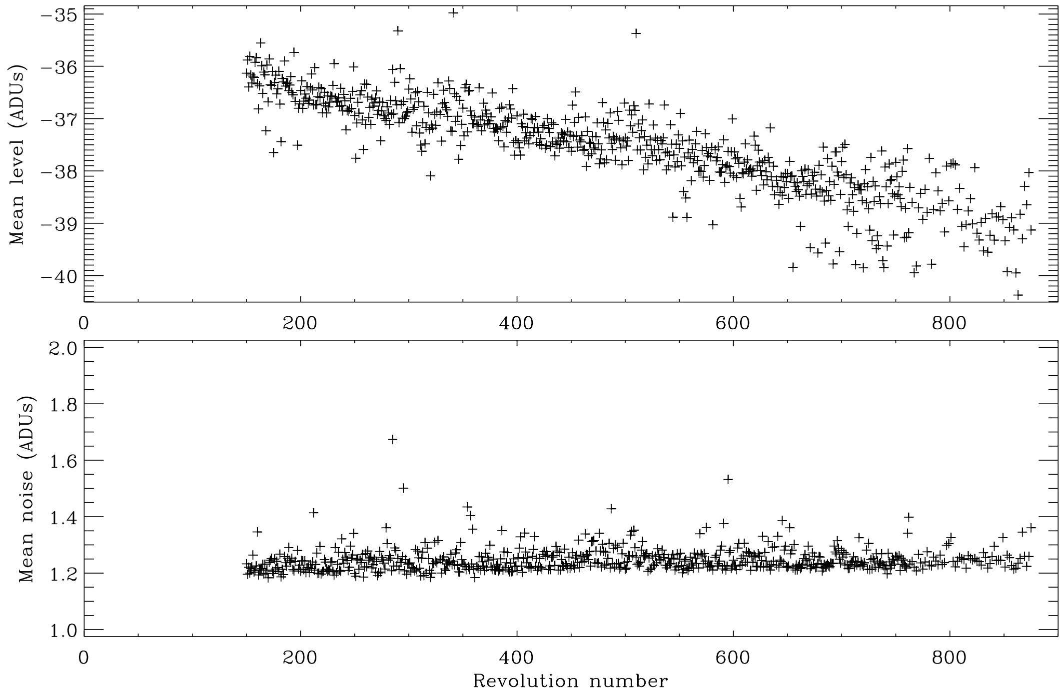


Figure 7: Hand-over LW 2 sec dark current measurements: mean level (top), mean temporal noise (bottom).

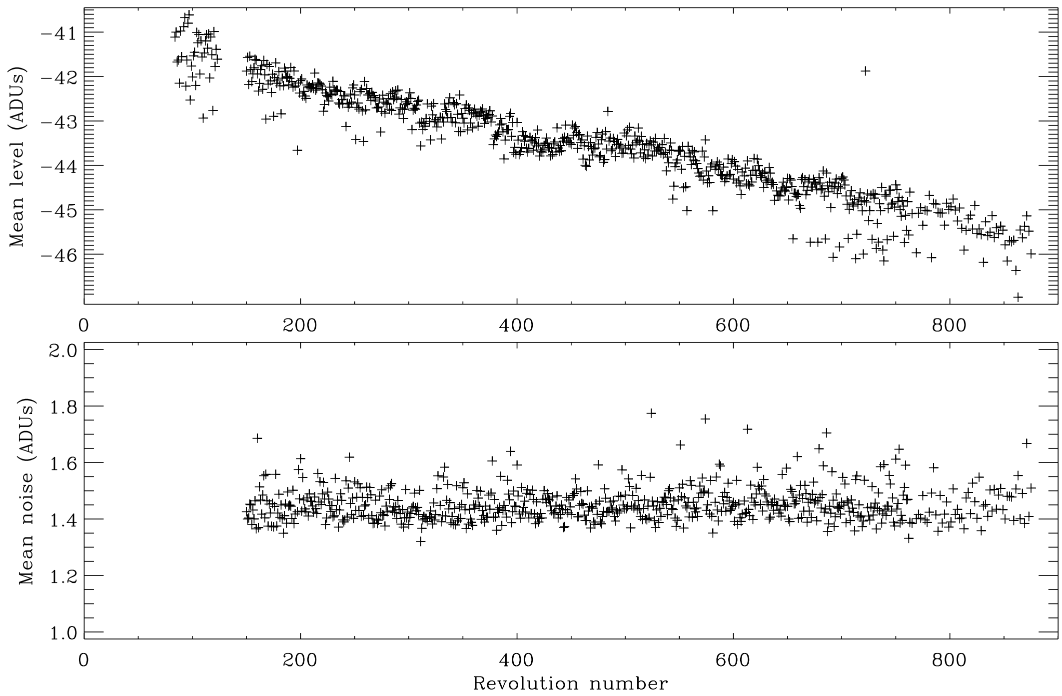


Figure 8: Hand-over LW 5 sec dark current measurements: mean level (top), mean temporal noise (bottom).

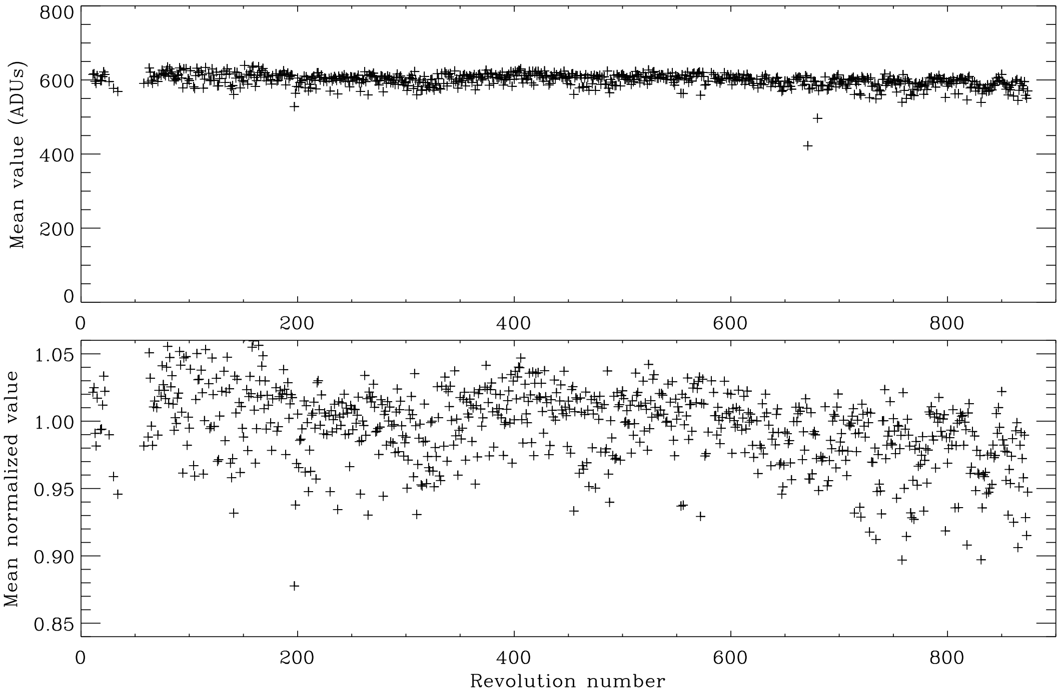


Figure 9: LW responsivity through the LW2 filter from deactivation measurements: mean level (top), mean normalized value (bottom).

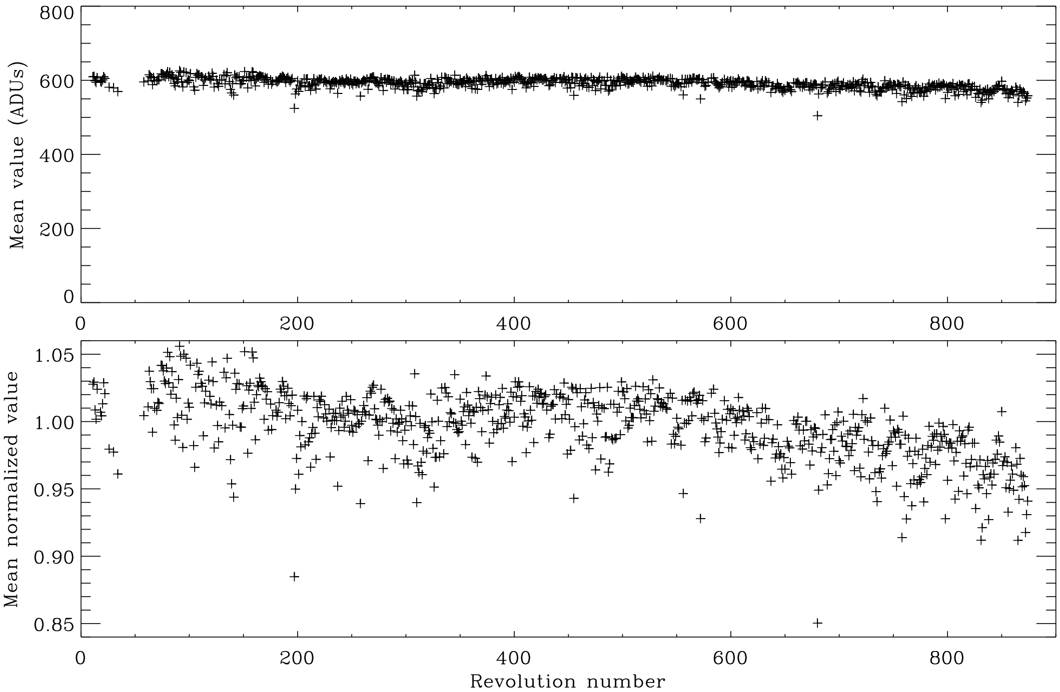


Figure 10: LW responsivity through the LW3 filter from deactivation measurements: mean level (top), mean normalized value (bottom).

# 4 On the use of the daily measurements

Daily dark current and flat-field measurements can not be used for direct calibration purposes. We present in this section, what we can learn from these measurements for the time being:

- CAM was sensitive to the space weather when the satellite was close to the radiation belts (see section 4.1).
- We possess a good statistical sample of flat-field measurements from which we can characterise the wheel jitter, already recognised in the science observations.
- End-of-revolution flat-fields hold the memory of any saturation events which occured during the revolutions. We can, with these measurements, recognise that part of the array where much care must be taken with regard to the photometry. This point is addressed in section 4.2.
- After ISO looked at the Earth, daily measurements have been of great interest to monitor the status and evolution of the instrument characteristics, and to see that no degradation of the detector occured (see section 4.4).
- Four times during the mission, CAM has been subject to a perturbation which is not yet understood, but which is seen through the mean RESET values of the LW detector as observed during dark current measurements (see section 4.5). As the RESET level is a reference level for the electronics, RESET values were affected as well as End-of-integration values, the drops are not seen in the difference frames.

## 4.1 The variations of the dark measurements

The long term trend analysis of the present calibration measurements shows a peculiar behaviour of the dark current measurements over a long time scale, for both detectors. This, seen only in the de-activation dark current measurements, is characterized by continuous variations of the level, from one revolution to the next. This is shown in figures 2, 3 and 6. The maximum value has been reached on revolution 452 (18-JAN-1997) where LW $t_i = 2\,\mathrm{sec}$ was greater than "nominal" by 20 ADUs/pixel, and SW $t_i = 6\,\mathrm{sec}$ was greater than "nominal" by 18 ADUs/pixel.

Having a look at the data, we note that:

- the variations are clearly dependant on the position along the orbit and are seen only in the de-activation dark measurements. It is clear from figures 7 and 8 that the hand-over measurements are not affected by any variation, as the de-activation dark measurements are.
- the variations seem to be independent of the channel. Both LW and SW dark currents are affected. Note that such similar behaviour has been observed by ISOPHOT, independently.
- No correlation with temperature variations is observed.
- The spatial distribution of the signal over the arrays seems to be homogeneous, just an offset is added to the mean signal over the whole array.

After having investigated in different directions, we found a good correlation between the dark current measurement values and the "space weather", i.e. the particle environment in the Earth's neighbourhood. On figure 6, we have plotted for comparison the LW dark current at $t_i = 2\,\mathrm{sec}$ against the $> 2\,\mathrm{MeV}$ electron fluence measured by the Space Environment Monitor (SEM) instrument package on board the Geosynchronous Operational Environmental Satellite (GOES) satellites (operating by the National Oceanic and Atmospheric Administration - NOAA). A set of data from this satellite, covering the period since 1st January 1996, has been kindly provided by D. Speich (Space Environment Center) and has been regularly dowloaded from the *Web* site[1] since August 1996.

However, the link between the measured dark levels and the electron fluence is not yet established, and the physical mechanisms are not yet understood. Because the LW RESET levels are not affected by such variation, the cause is not linked to any variation of the gain of the electronic chain. So then the explanation may be an extra signal directly recorded by the detectors. This is confirmed by the fact that the relation between the extra signal on the detectors, expressed in electrons/second, does not follow a linear law (see fig. 11).

A more detailed analysis is needed to explain clearly this phenomenon, taking into account the location of ISO on its orbit in regard to the GOES spacecraft, the dimensions of the detectors, and their intrinsic characteristics such as gain and quantum efficiency.

[1] `gopher://proton.sec.noaa.gov:70/00/latest/DPD`

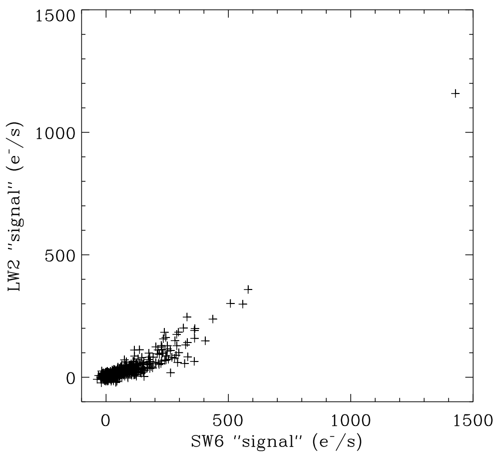


Figure 11: SW additional signal in terms of electrons per second against the same quantity for the LW detector.

## 4.2 Wheel jitter

As seen in section 3.1.2, the SW flat-field measurements present a multi-modal distribution both through the SW1 and SW3 filters.

This phenomenon can be explained by a combination of different repositioning uncertainties of some wheels in the gearwheel, following an optical reconfiguration of the camera. It affects both LW and SW measurements.

Assuming that the median flat-field measurement derived from the whole set of measurements is the ideal flat-field, then we can correct each individual image for the pixel-to-pixel response variation. At the end of this operation, the images are not as flat as we could expect. They display a clear circular pattern which can be attributed to a change of the position of the centre of the illumination field in the images.

The multi-modal distribution is well seen in the case of the images obtained during the deactivation flat-field measurement of the SW detector through the SW3 filter (see figure 12, (the signals have been corrected for the general drift of the response).

Because a circular pattern, moving in the horizontal direction of the image ($y$ axis of the spacecraft) is observed, we can consider the left and right parts of the detector for the analysis.

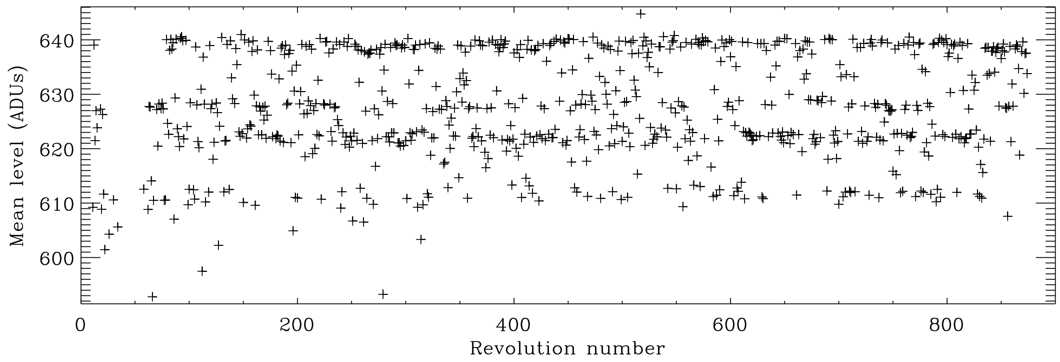


Figure 12: Mean level on SW detector of flat-field measurements through the SW3 filter obtained during de-activation sequence.

In figure 13, we plotted, in the case of the flat-field measurement through SW3 during deactivation, the mean signal over the left part of the detector minus the mean signal over the right part of the detector against the mean signal over the whole array: points are clearly distributed over 8 well defined regions of the plot.

In order to characterize each family of points, and to establish the physical links which can exist between families, we derived, for each set of points, a median image representative of the group. Among the 4 main families identified in figure 12 (named Fam1, Fam2, Fam3 and Fam4) and which clearly appear, 2 of them (Fam2 and Fam4) are split in 3 groups depending on the level of the difference between their right and left parts (Fam2a,b,c and Fam4a,b,c).

The median images for each group are displayed in figure 14, together with the image ratios of linked families. The images of the signal show that the center of illumination is displaced along a sequence depending on the difference left-minus-right. The 2 sequences of evolution are: Fam1, Fam2a, Fam2b and Fam2c for the first sequence and Fam3, Fam4a, Fam4b and Fam4c for the second sequence. Along these sequences, and in similar ways, the center of illumination is moving from the left to the right, i.e along the $-y$ axis of the spacecraft.

For 2 values of the difference left-minus-right, the image ratios show the same pattern in the 2 sequences. A displacement of the center of the illumination field is evident. This displacement being done in the $y$ axis direction, a poor reproducibility of the selection wheel position due to play in the gear, favouring four positions, could explain this result. We notice that even if these privileged positions of the wheel exist, intermediate positions seem to occur, and these invite us to link Fam1 to Fam2 and Fam3 to Fam4.

In another way, each couple of families which have the same difference left-minus-right display the same kind of pattern. For instance, for Fam1 and Fam3, the pattern is vignetted on the right, while for Fam2c and Fam4c, the pattern is vignetted on the left. We can then define 4 couples of families: (Fam1, Fam3), (Fam2a, Fam4a), (Fam2b, Fam4b) and (Fam2c, Fam4c), and the ratios of the images in a each couple are similar for the 4 couples. The similarity indicates that another effect is contributing to the observed multi-modal distribution of SW response throughout the mission. The derived pattern does not allow one to clearly identify the origin of the bimodal distribution. Can this pattern be linked to a displacement of the lens wheel due to play in the gear (because its movement displaces images in the $z$ axis direction) leading to a variation of the illumination field on the detector ? In fact, this last effect is responsible for the quadri-modal distribution initially observed.

Now, we have at our disposal a set of 8 images representative of the combinations of the different basic patterns. These images can be used on the whole set of measurements of the SW responsivity for comparison, associating one of the 8 images with each image obtained during the ISO mission, the criterion of selection being the minimisation of the spatial noise of the image ratio. This has been done and the results are displayed on figure 15. After comparison, the multi-modal distribution of points disappeared and the dispersion has been reduced from 4.1% (global dispersion) to 0.6% (in the central peak, the same as the dispersion measured in each individual peak before correction).

We made the same kind of analysis for the LW flat-field measurements. As for measurements of the SW channel, measurements of the LW channel are also affected by wheel jitter. This effect is seen in figure 16, where we plotted the mean signal over the array against the difference between the mean value on the left part and the mean value on the right part of the detector. The points are more scattered than the SW ones on this kind of graph. Using the same method as used in the SW case, we derived 4 families of points. These images and the ratio between images are displayed in figure 16. The ratio between each family member shows clearly a pattern which corresponds to a move of the center of illumination produced by the poor reproducibility of, in this case, one wheel. Because the move is observed in the $y$ direction, the concerned wheel is certainely the selection wheel.

A poor reproducibility of the selection wheel due to play in the gear has previously been observed in science data, on the edge of the Fabry mirror: in these data, either the first or the last column can be vignetted. A detailed modelling, taking into account the optical gemetry of the camera, could provide an estimation of the effects of the play of the gear on the movement of the pattern in the focal plane.

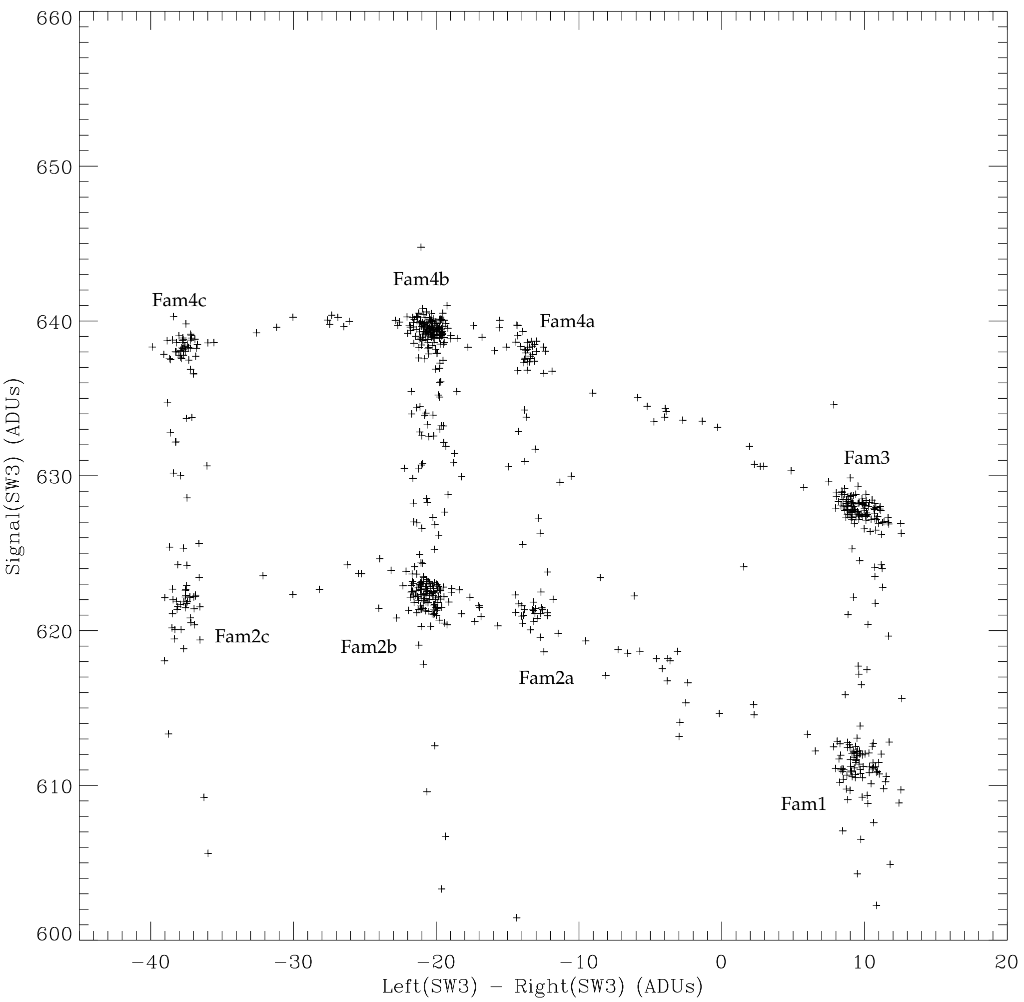


Figure 13: SW deactivation flat-field: Mean value over the SW array versus difference between the left part of the detector and the right part of the detector ($y$ axis of the satellite is oriented from right to left).

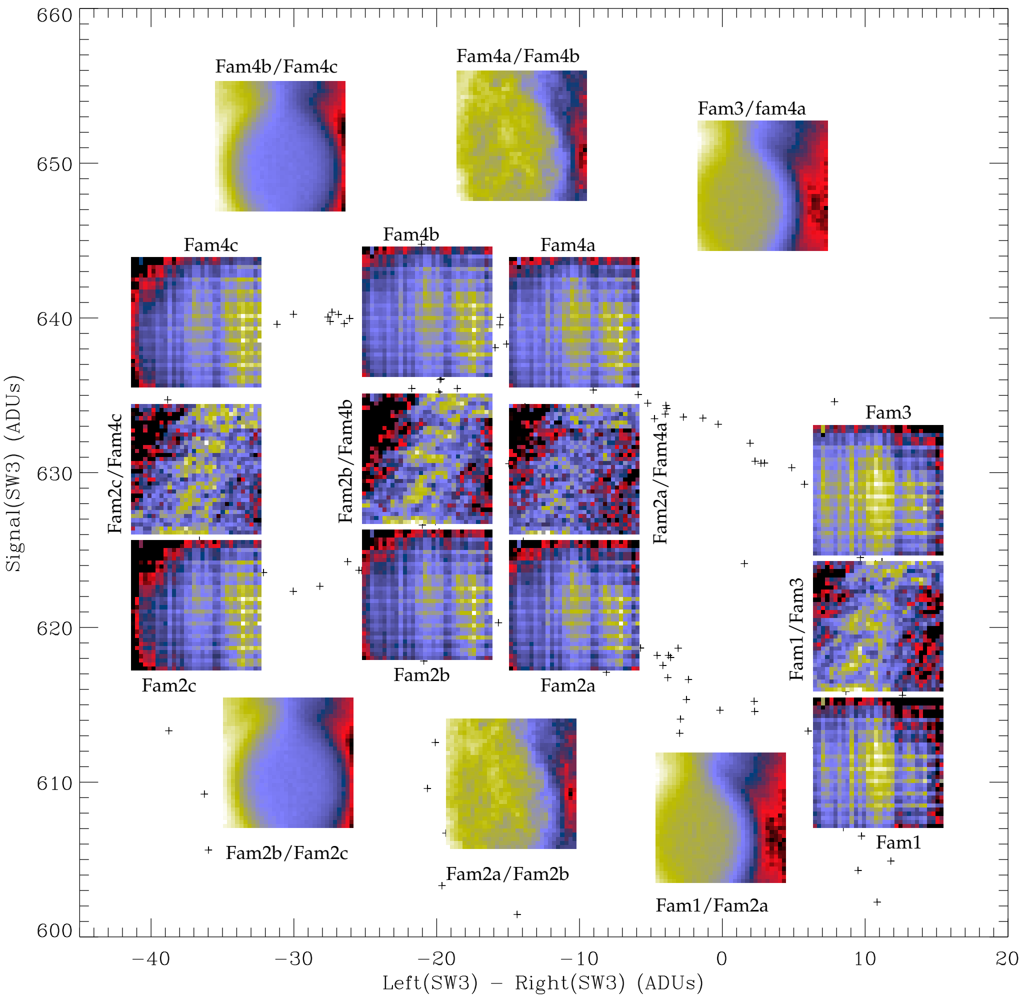


Figure 14: SW deactivation flat-field: same plot as figure 13 in which we superimposed the images of the ICD illumination and the image ratios between couples of families.

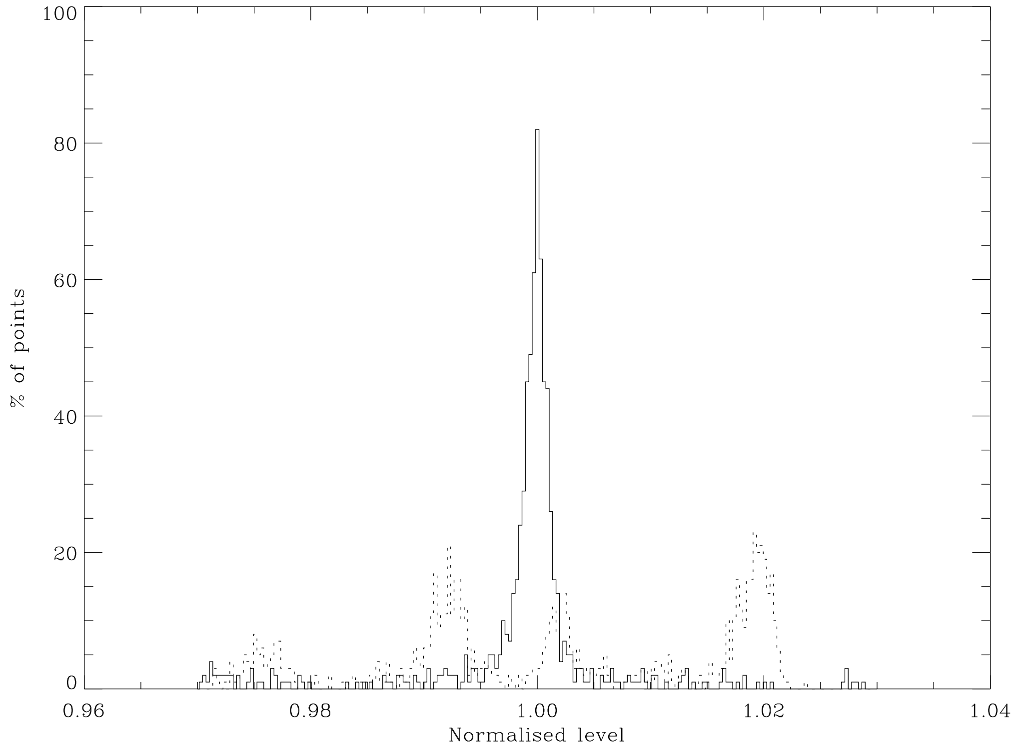


Figure 15: Histogram of the distribution of mean signal of flat-field measurements (corrected for drift) before (dotted line) and after (full line) correction for wheel jitter.

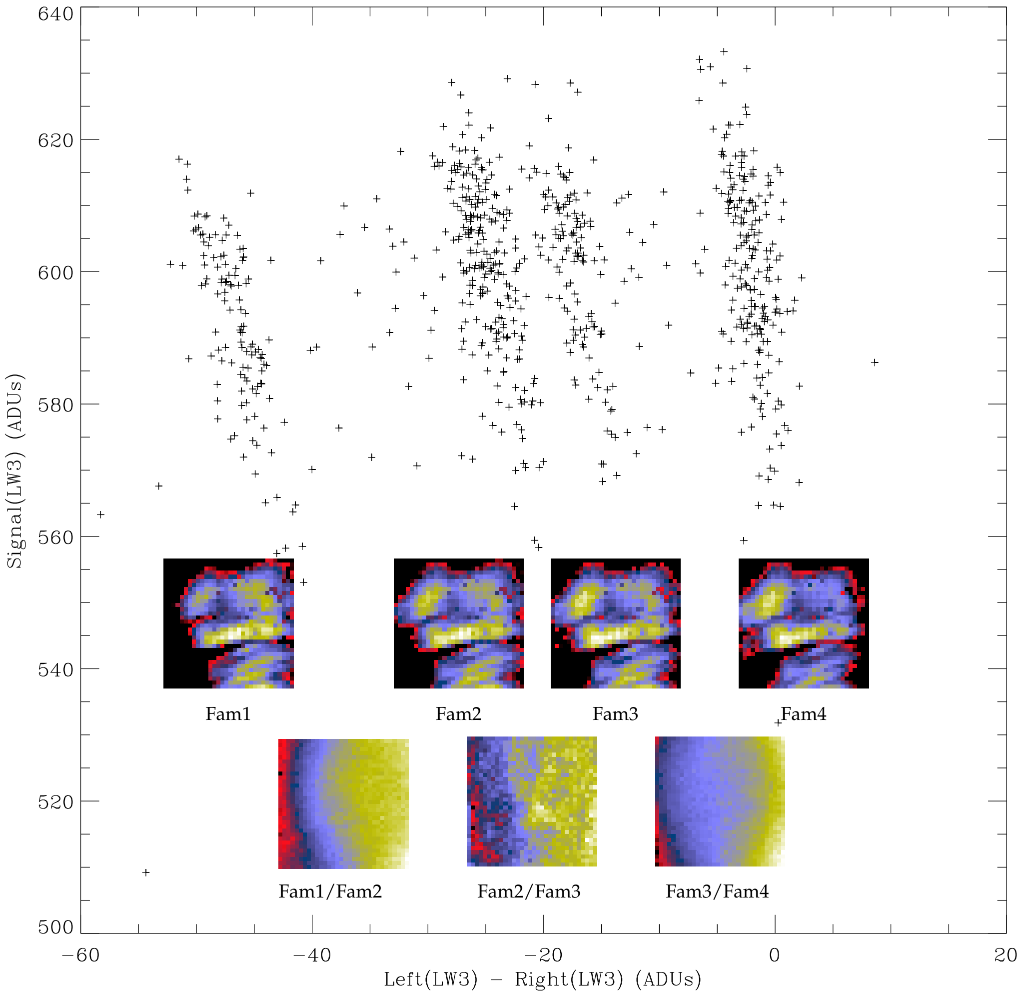


Figure 16: LW deactivation flat-field measurements: Mean value over the LW array against difference between the left part of the detector and the right part of the detector ($y$ axis of the satellite is oriented from left to right). The images of the ICD illumination for each family of points and the image ratios between couples of families are also displayed.

## 4.3 Saturation effects

For the LW detector, the main effect of a saturation is a decrease of the responsivity of that part of the array which has been illuminated by a too high flux level. It is currently seen in science observations in the form of an undesirable remnant of any bright source, appearing as a hole compared to the level of the neighbouring background. If no curing of the detector is performed after a saturation event, as was usually the case during ISO operations because of the time constraints, we can observe this remnant a long time after the triggering event, and the affected pixels can take hours, even days to recover their nominal responsivity. As the effect of the decrease of the responsivity can be observed when the detector is “homogeneously” illuminated, flat-field measurements, such as those performed during the de-activation sequence are well suited to identifing any serious event which could have occurred inside the revolution and which could have left a trace on the detector. On figure 17, we give as an example a gallery of patterns seen in the ICD measurements, and the origin of the pattern.

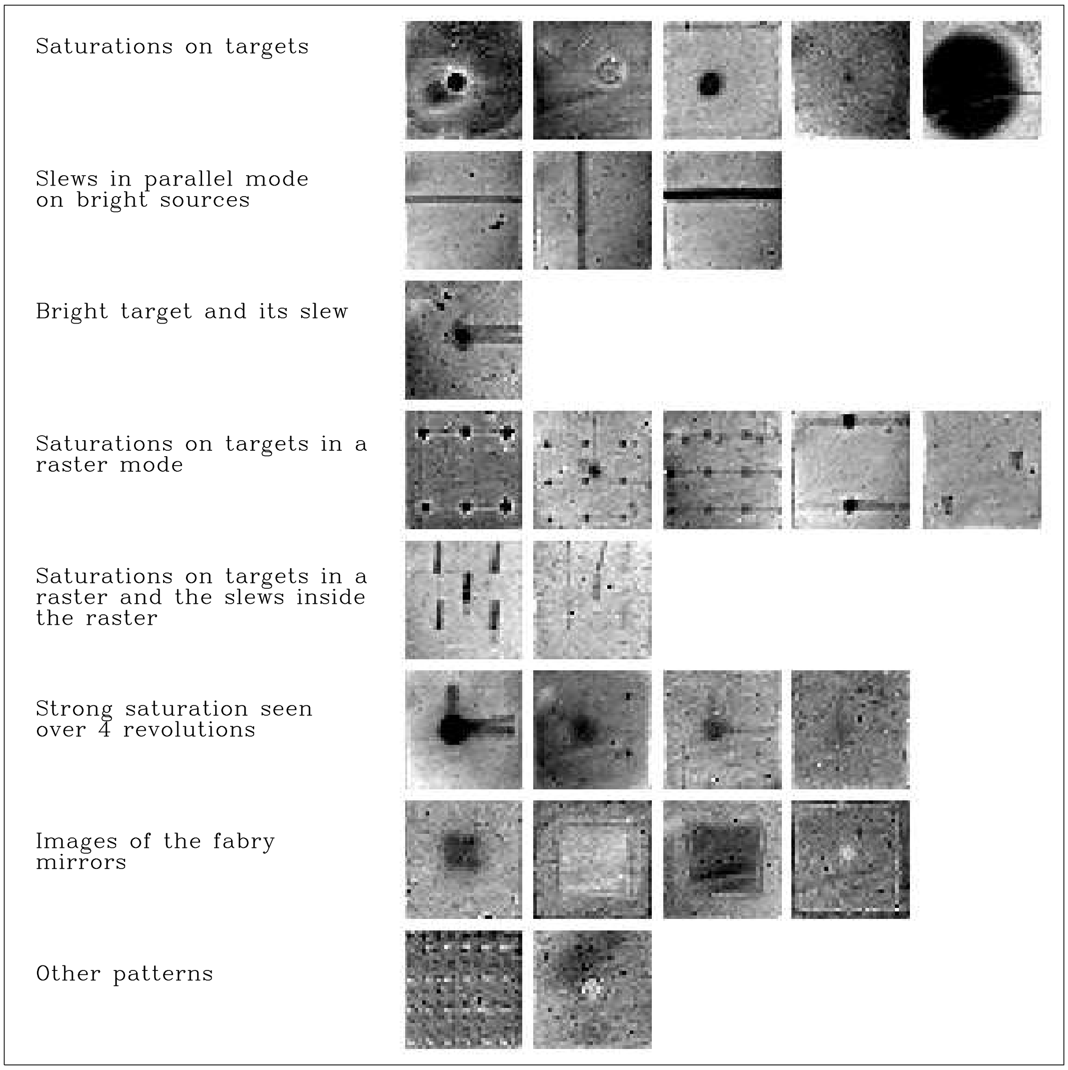


Figure 17: Gallery of LW saturation remnants.

Normally, the passage through the proton radiation belts, followed by the curing of the detector during the activation sequence, remove the remnants. However, for a large fraction of saturation events, this has not been the case. This can be seen in the images we obtain at the end of the activation flood.

During operations and for quality check purposes, ICD measurements were intensively monitored to qualify the strength of saturation events. Of course, if the responsivity of a pixel, or of a part of the array, is less than nominal, photometry of any sources observed by these pixels must be considered very carefully. For this purpose, we supply, in annex A, the set of normalised ICD measurements through the LW2 filter for the whole ISO mission. Then, the observer can refer to this library of deactivation flat-fields and check whether the flat-field measurement done during a given revolution shows any saturation remnant.

## 4.4 Consequences of the revolution 196 problem

At the end of revolution 195, during perigee passage, ISO violated the Earth constraint, leading to an increase of the temperature of the OSS. CAM, like the other instruments, was switched off during the whole revolution 196. During the first part of revolution 197, CAM was switched on and a manual deactivation was performed in order to get an idea of the consequences of the high temperature of the OSS on the CAM responsivity.

After this event, the responsivity clearly decreased by about 7% for the SW channel and about 15% for the LW channel

Dark current measurements have shown also a decrease, values being lower (!) than "usual" by 2 ADUs both LW $t_i = 2$ sec and $t_i = 5$ sec integration times, and about 5 ADUs for SW $t_i = 6$ sec measurements.

Responsivity for both detectors recovered well since about revolution 200, and the violation of the Earth constraint has had no consequences - neither on the behaviour of ISOCAM nor on its performance.

## 4.5 About the LW RESET levels

Together with the basic parameters (dark current and responsivity), we monitored also the so-called RESET level of the LW detector. This parameter corresponds to the reference electronic level before integration of charges in the detector itself, i.e. to the level of the pixel after the controlled setting of some bias of electronic components to a defined value once the read-out of the detector has been performed. To obtain a final image, we must take the difference between the end-of-integration (hereafter EOI) frame and the associated RESET frame. We extracted then the value of this parameter when the detector did not see any light, i.e., during the dark current measurements. Note that the definition of RESET is not the same for the SW detector and in that case it is not relevant to the present discussion.

Mean values of the RESET levels along the ISO mission for the de-activation dark current measurements are shown on figures 18 and 19. From these plots, we can notice 2 features: first, the general tendancy of the mean value to decrease with time, and second, the strong drops followed by a slow recovery to the nominal level.

### 4.5.1 General trend

The RESET level shows a different trend relative to the dark current. It decreased by about 25 ADUs (i.e. $\sim$ 0.24% per 100 revolutions) over the whole ISO mission, while the dark current level itself decreased by $\sim$ 3 ADUs (i.e. $\sim$ 1% per 100 revolutions). This difference shows that the evolution of the electronics in time is different from the evolution of the detector alone.

### 4.5.2 Events

On four occasions the RESET level showed a strong drop followed by a slow recovery to the nominal level. These events are not yet understood. It is clear that the electronics suffered from external events.

No such variation of any measured bias levels of the camera has been seen up to the present time. High proton fluence has not been observed in the same periods.

One possible explanation could be the consequences of sudden electrostatic discharges of the whole spacecraft which can produce spikes in the electronics (see Evans, 1998). This idea should be the subject of a deeper analysis. The observed events occured around revolutions 86 (11 Feb. 1997), 310 (22 Sep. 1997), 556 (25 May 1997), and 753 (8 Dec. 1997), between the hand-over window and the de-activation window for the last three. The time between two events is quite periodic ($\sim$ 205 to 247 days) and the discharging of the spacecraft can occur periodically, depending of course on the level and variation of the electrostatic potential along the orbit producing the surface charging of the spacecraft.

Because the RESET level is defined as a reference level after read-out of the detector, its variation should not affect the resulting difference image.

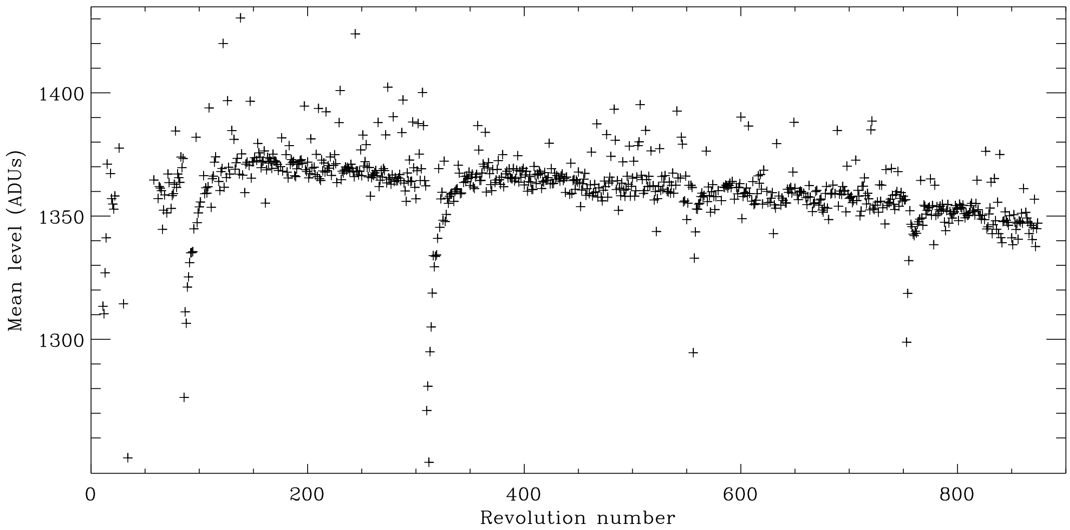


Figure 18: Mean value of the LW RESET value during deactivation LW 2sec dark current measurements.

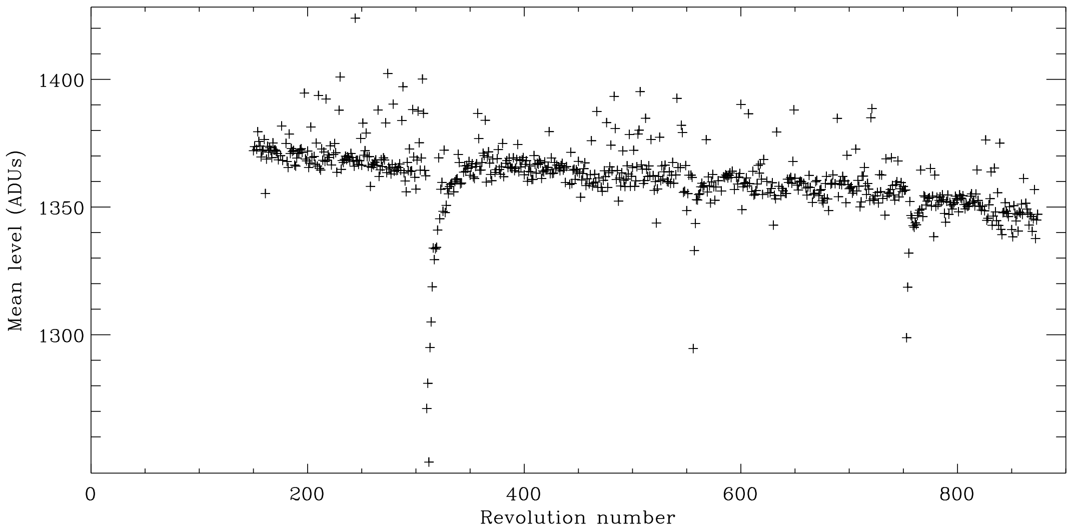


Figure 19: Mean value of the LW RESET value during hand-over LW 2sec dark current measurements.

# 5 Conclusions

This report does not make pretention to explain all problems, features or behaviour observed during the handover and de-activation windows. It shows the diversity of information we can obtain about the behaviour of the instrument, with its detectors, in the in-flight operational environment. It shows also the importance of monitoring at a good frequency, not only the system parameters, but also, the detector characteristics.

CAM, and its detectors, performed nominally during this extended space mission.

# 6 References


- Biviano A. et al, 1998, in proceedings of the *ISO Detector Workshop*, held at Villafranca (Spain) in January 1998, in press.
- Evans H., 1998, *Space Radiation Environment during ISO Mission*, April 9, 1998, Esa ref. esa/estec/ema/he/ISO/98-1.
- Boulade O. and Gallais P., 1998, in proceedings of the *ISO Detector Workshop*, held at Villafranca (Spain) in January 1998, in press.
- Delaney et al, 1998, *ISOCAM Interactive Analysis User's Manual*, version 2.5, June 7, 1998, ESA ref. SAI-96-5226/Dc

# Annex A: Gallery of LW images

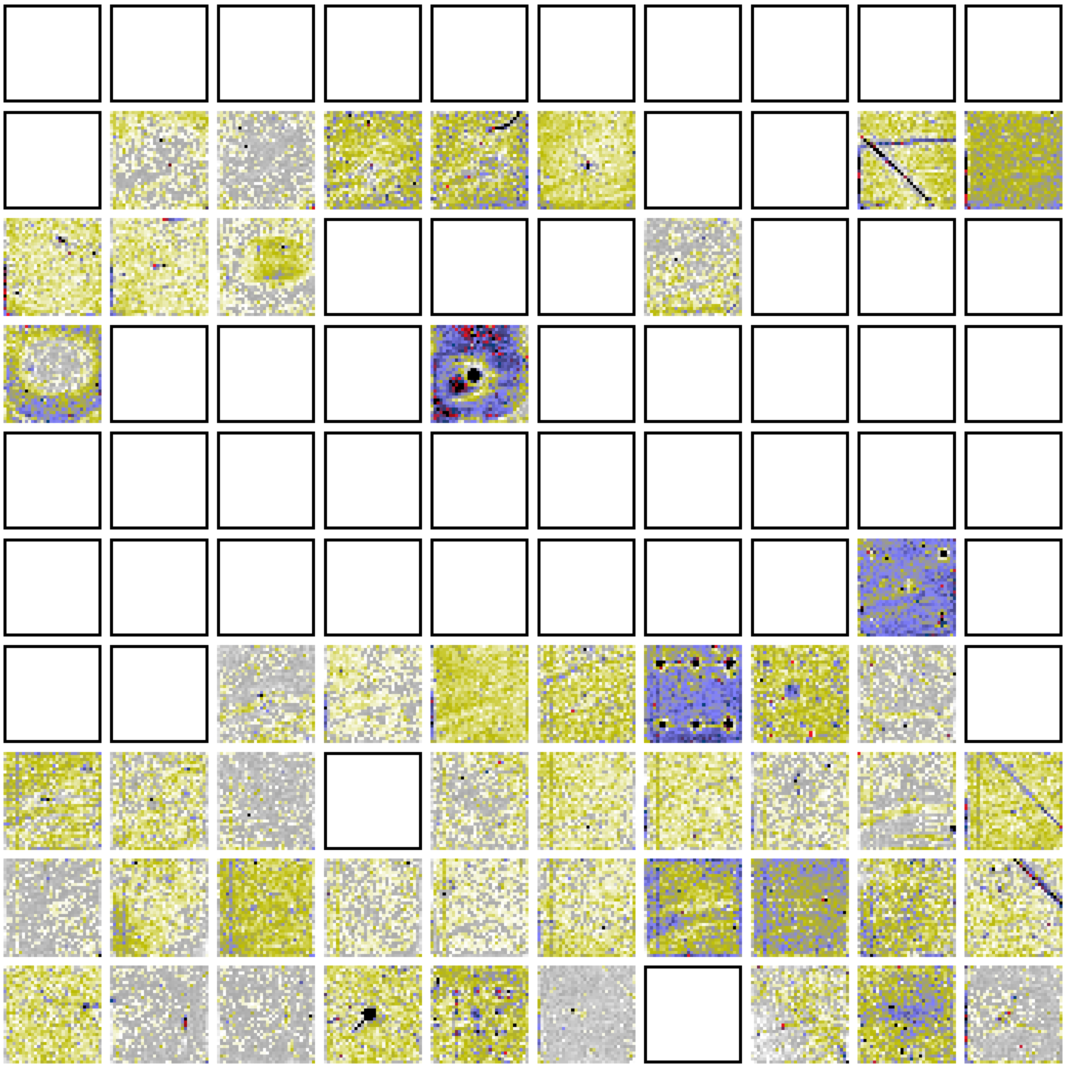

Figure 20: Normalised LW flat-field at the end of revolution, for revolutions 0 to 99.

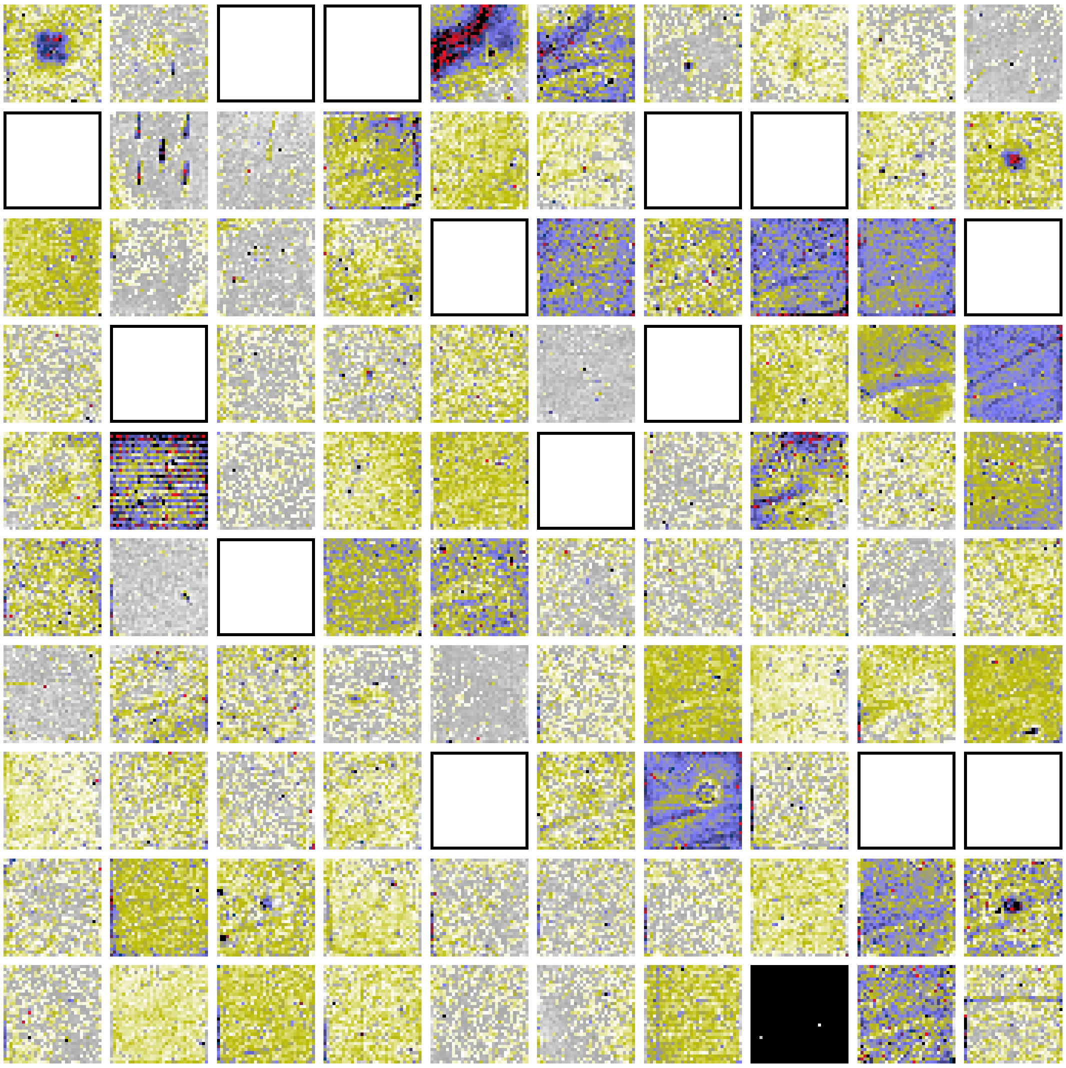

Figure 21: Normalised LW flat-field at the end of revolution, for revolutions 100 to 199.

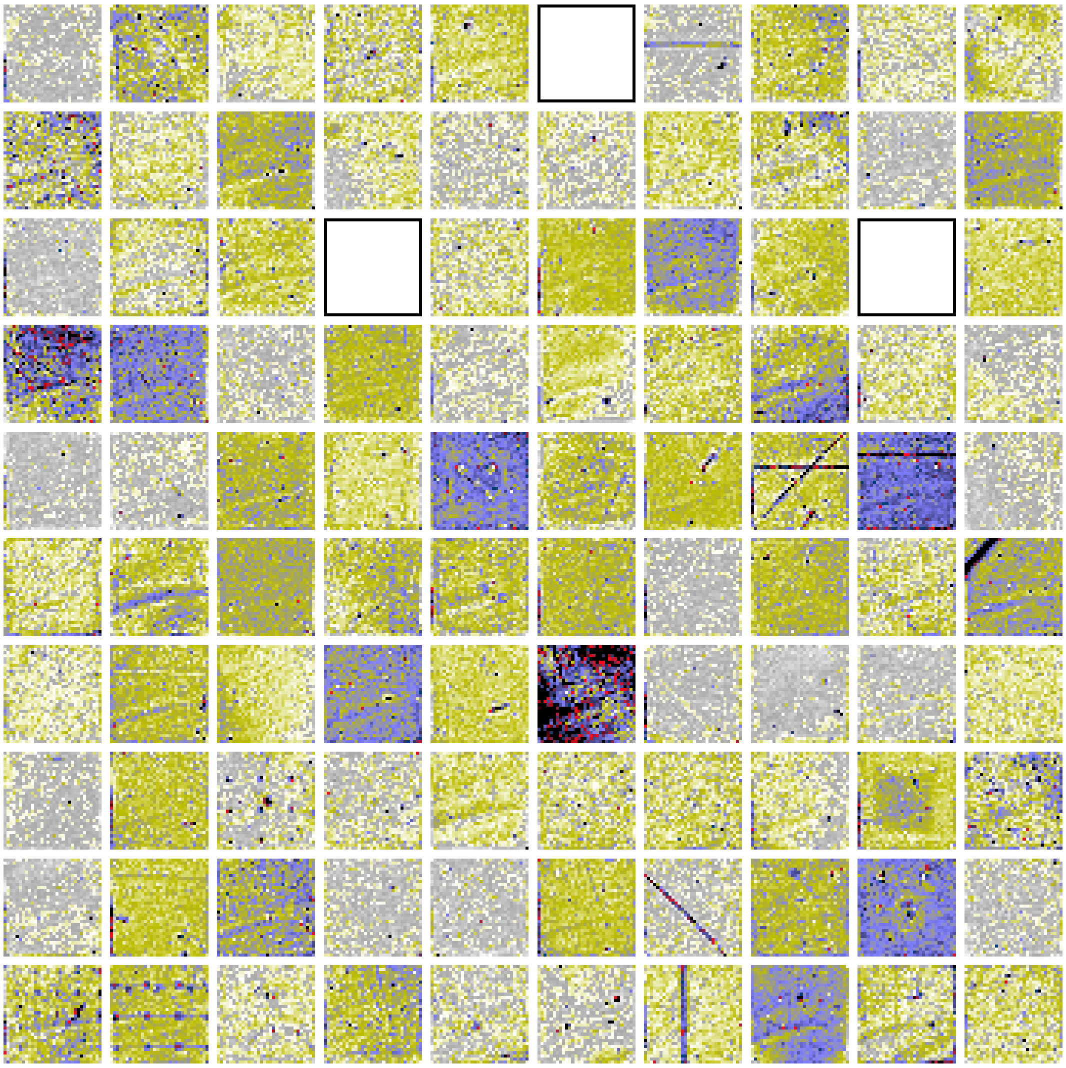

Figure 22: Normalised LW flat-field at the end of revolution, for revolutions 200 to 299.

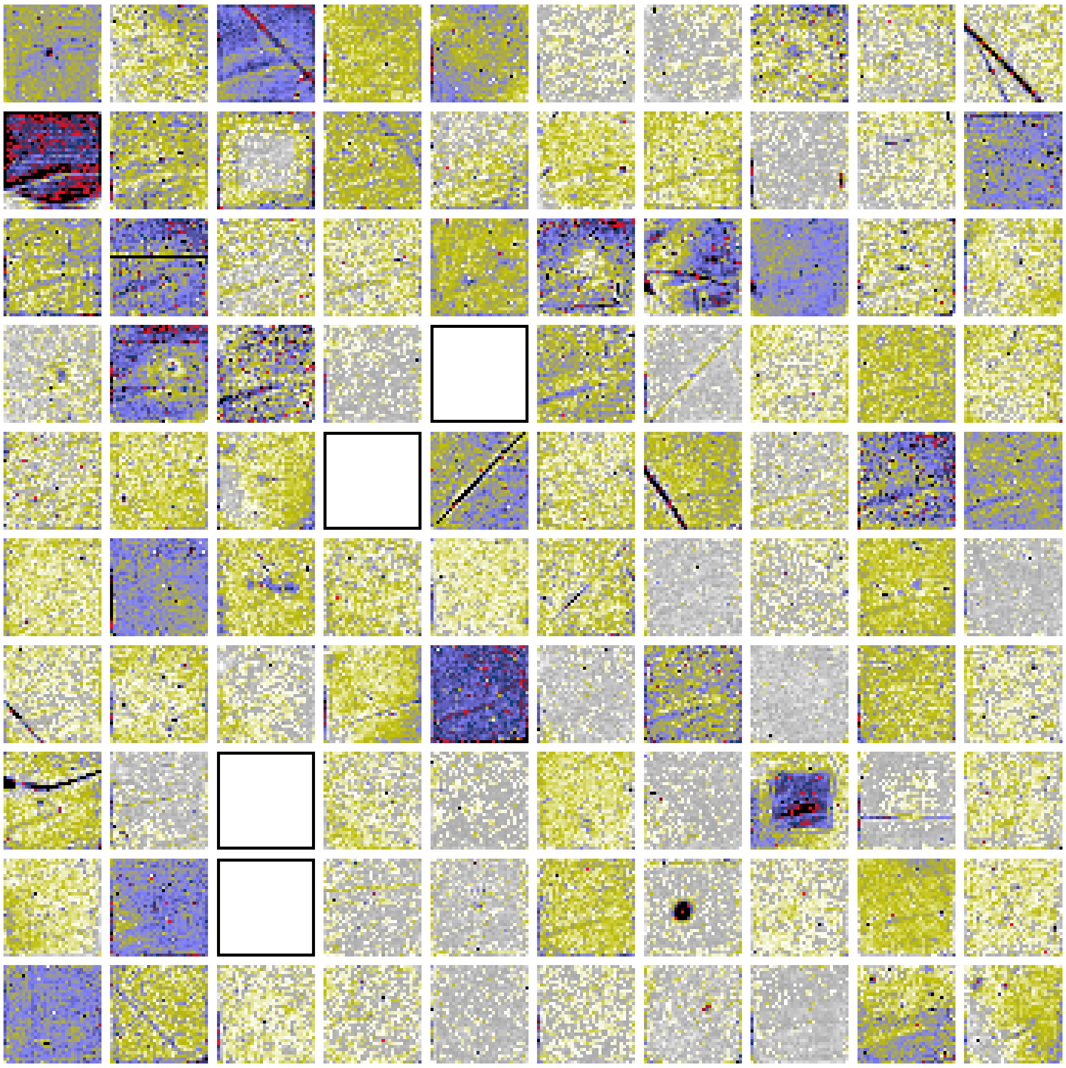

Figure 23: Normalised LW flat-field at the end of revolution, for revolutions 300 to 399.

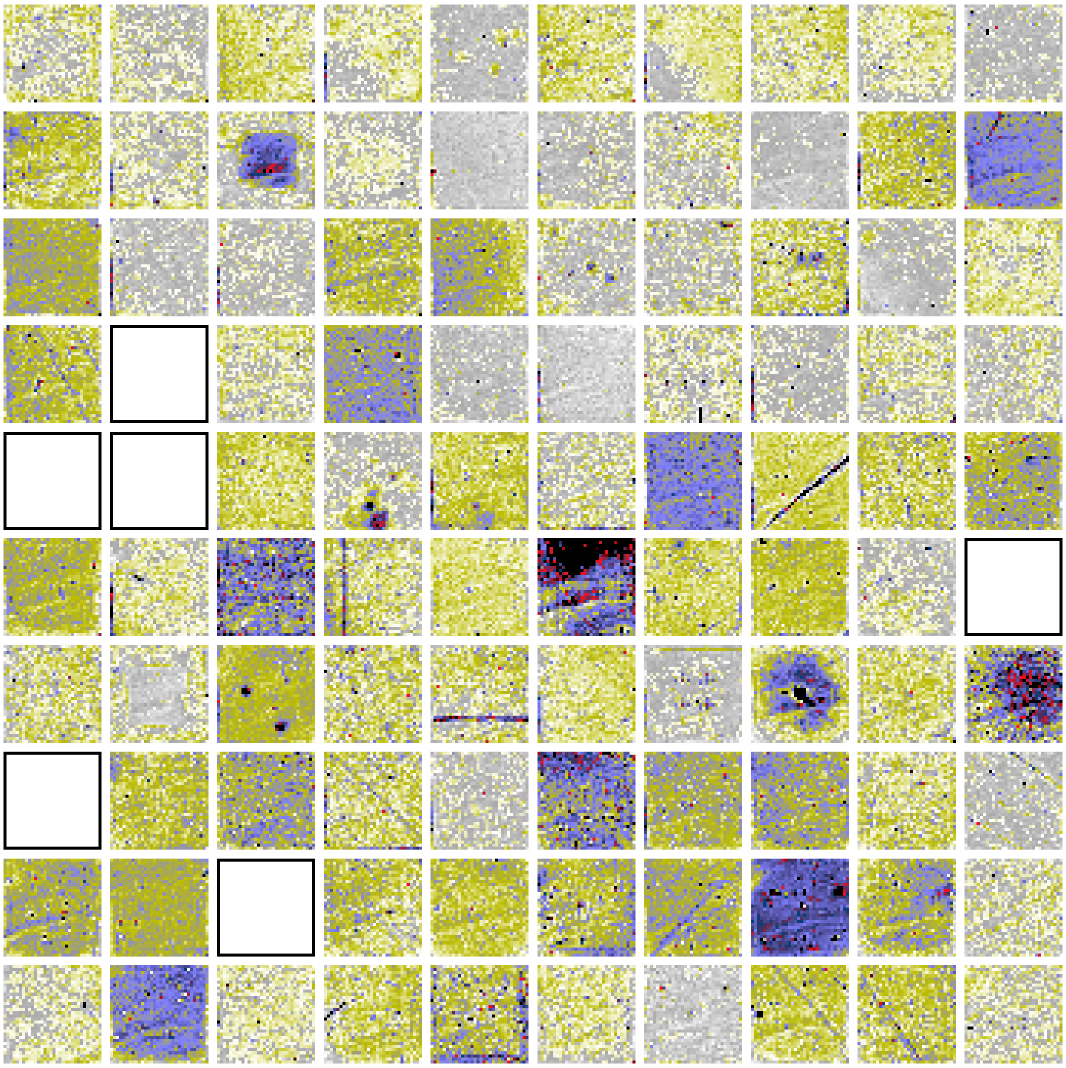

Figure 24: Normalised LW flat-field at the end of revolution, for revolutions 400 to 499.

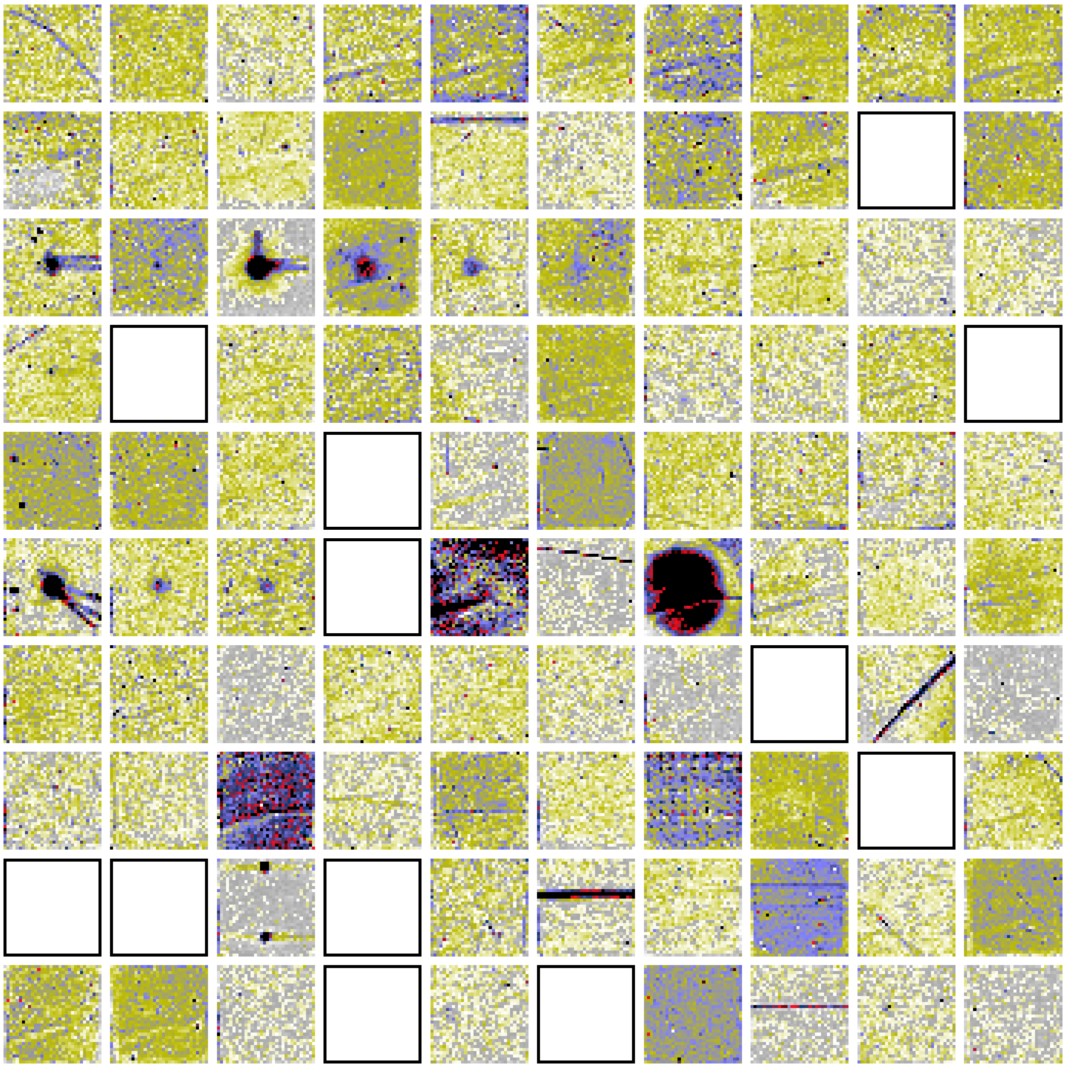

Figure 25: Normalised LW flat-field at the end of revolution, for revolutions 500 to 599.

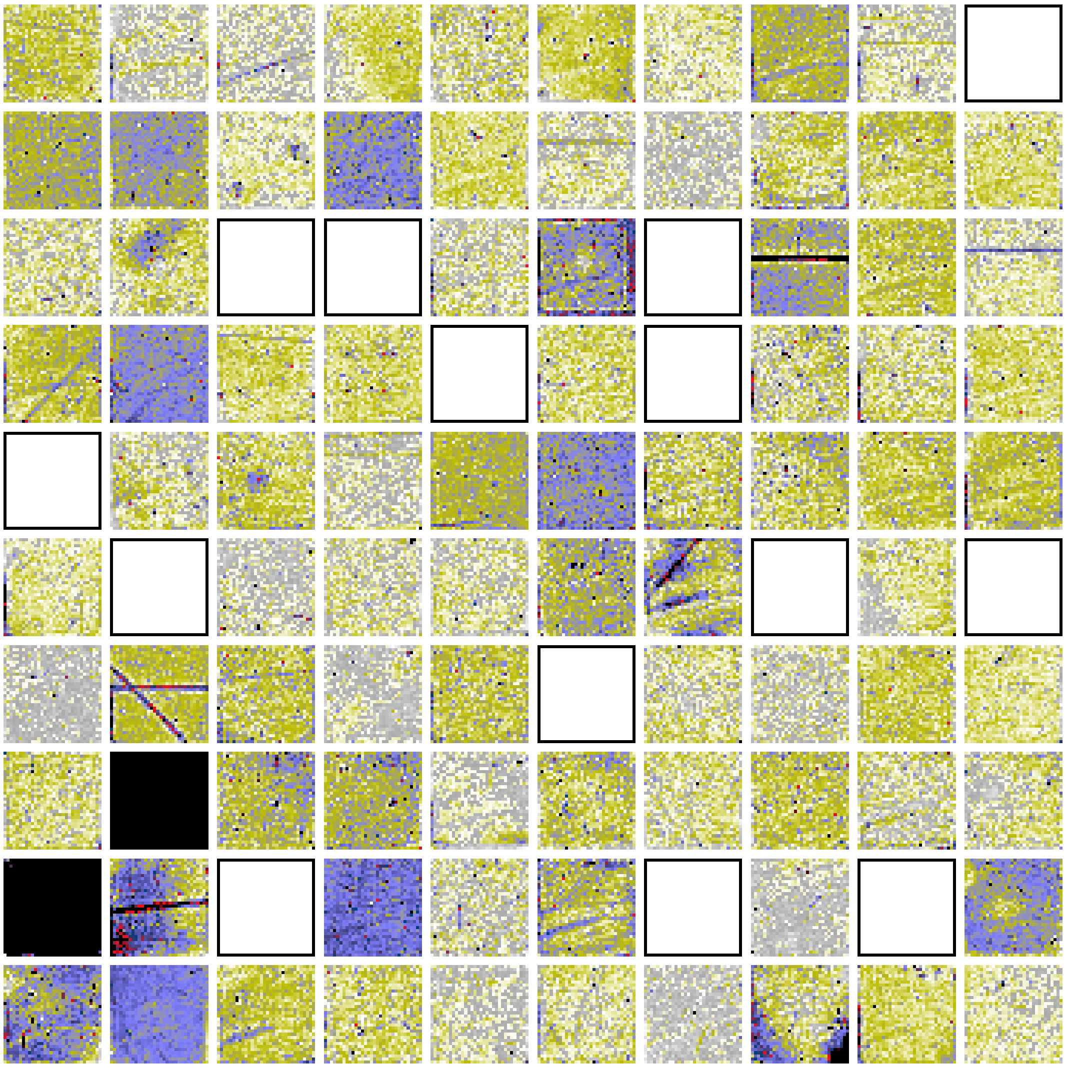

Figure 26: Normalised LW flat-field at the end of revolution, for revolutions 600 to 699.

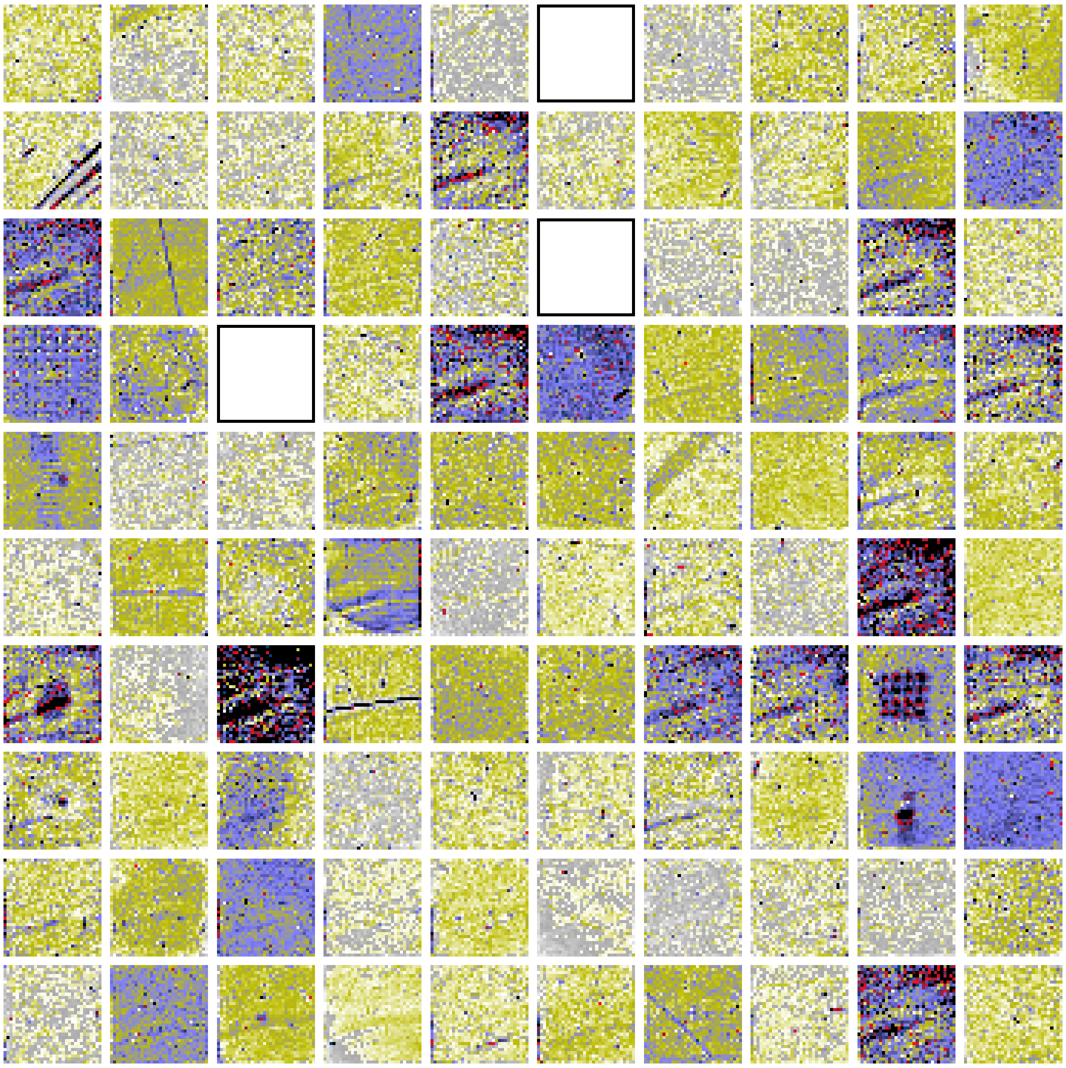

Figure 27: Normalised LW flat-field at the end of revolution, for revolutions 700 to 799.

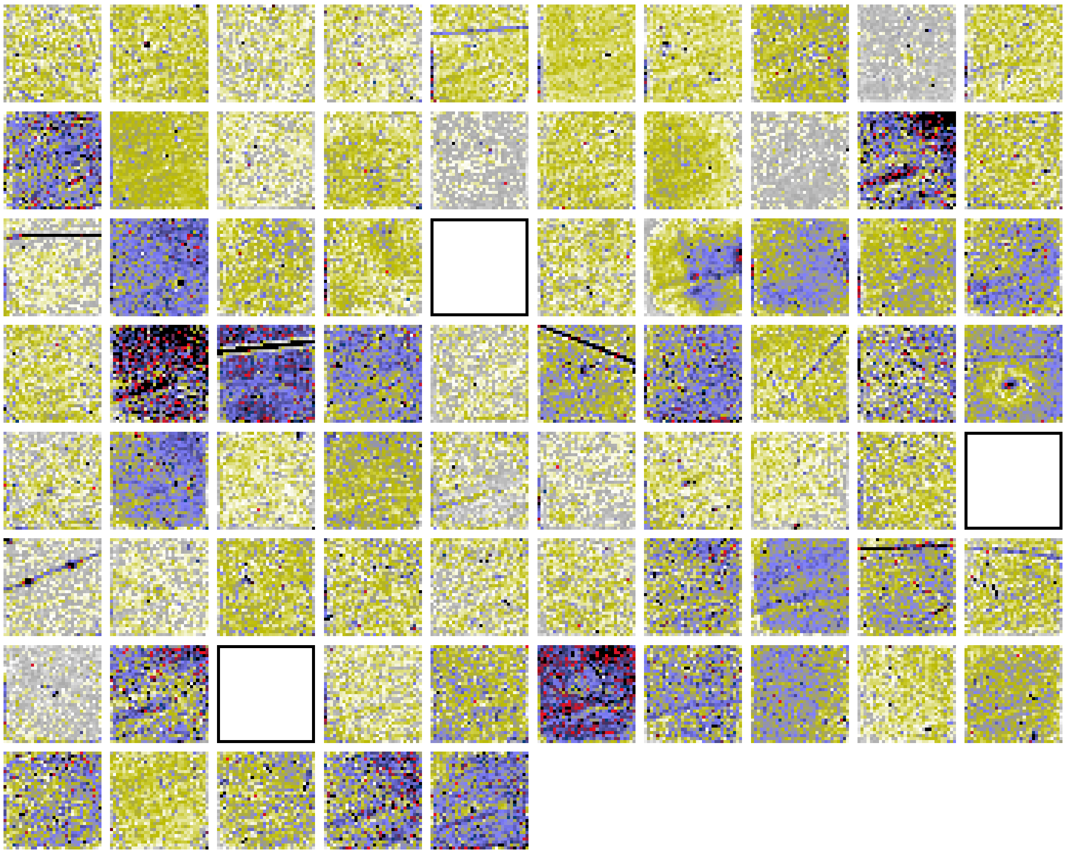

Figure 28: Normalised LW flat-field at the end of revolution, for revolutions 800 to 875.